PTEP

Prog. Theor. Exp. Phys. **2015**, 063E01 (16 pages)
DOI: 10.1093/ptep/ptv072

Effects of triple-α and $^{12}C(\alpha, \gamma)^{16}O$ reaction rates on the supernova nucleosynthesis in a massive star of 25 $M_{\odot}$

Yukihiro Kikuchi, Masa-aki Hashimoto*, Masaomi Ono, and Ryohei Fukuda

Department of Physics, Kyushu University, Fukuoka 812-8581, Japan
*E-mail: hashimoto@phys.kyushu-u.ac.jp

Received October 28, 2014; Revised April 20, 2015; Accepted April 22, 2015; Published June 8, 2015

We investigate the effects of triple-α and $^{12}C(\alpha, \gamma)^{16}O$ reaction rates on the production of supernova yields for a massive star of 25 $M_{\odot}$. We combine the reaction rates to examine the rate dependence, where the rates are considered to cover the possible variation of the rates based on experiments on the earth and on theory. We adopt four combinations of the reaction rates from two triple-α reaction rates and two $^{12}C(\alpha, \gamma)^{16}O$ ones. First, we examine the evolution of massive stars of 20 $M_{\odot}$ and 25 $M_{\odot}$ whose helium cores correspond to helium stars of 6 $M_{\odot}$ and 8 $M_{\odot}$, respectively. While the 25 $M_{\odot}$ stars evolve to the presupernova stages for all combinations of the reaction rates, the evolutionary paths of the 20 $M_{\odot}$ stars proceed significantly differently for some combinations, which are unacceptable for progenitors of supernovae. Second, we perform calculations of supernova explosions within the limitation of spherical symmetry and compare the calculated abundance ratios with solar system abundances. We can deduce some constraints to the reaction rates. The results show that a conventional rate is adequate for a triple-α reaction rate and a rather higher value of the reaction rate within the upper limit for the experimental uncertainties is favorable for a $^{12}C(\alpha, \gamma)^{16}O$ rate.

Subject Index D40, E25, E26

1. Introduction

The triple-α (3α) and $^{12}C(\alpha, \gamma)^{16}O$ reactions play a crucial role in helium (He) and carbon (C) burning stages in the evolution of low-, intermediate-, and high-mass stars [1–3], and accreting compact stars [4–6]. The 3α reaction rate calculated by Ogata et al. [7] (hereafter the OKK rate) is very large compared with previous rates [6,8] for temperatures below 2×10^8 K. The rate from Fynbo et al. [9] (Fynbo rate) which revised the 3α rate of Ref. [8] is based on new experiments at a high temperature of $T > 10^9$ K. The ratios of the OKK rate to the Fynbo rate are 1.0, 1.9, 1.5×10^6, and 3.6×10^{26} for $T_8 = 2.5$, 2, 1, and 0.1, respectively (T_8 is temperature in units of 10^8 K). The OKK rate is shown in Fig. 1, where the representative rates obtained so far are compared. It is noted that a conventional formula $\dot{y}_{12} = -1/6\rho^2 N_A^2 \langle\alpha\alpha\alpha\rangle y_4^3$ with the abundance $y_i = n_i/(\rho N_A)$ is used, where n_i is the number density of a nucleus i ($i = 12$ for ^{12}C and $i = 4$ for ^{4}He), ρ is the mass density, and $N_{\rm A}$ is the Avogadro constant [6]. We must investigate how the new rates affect the astrophysical phenomena, because terrestrial experiments for the 3α reaction are very difficult.

The uncertainty of the rate of the $^{12}C(\alpha, \gamma)^{16}O$ reaction is known to be within a factor of two from nuclear experiments [11,12]. Direct measurements of this reaction are very difficult for the low-energy region corresponding to the stellar energy of 300 keV at which we need the cross section.

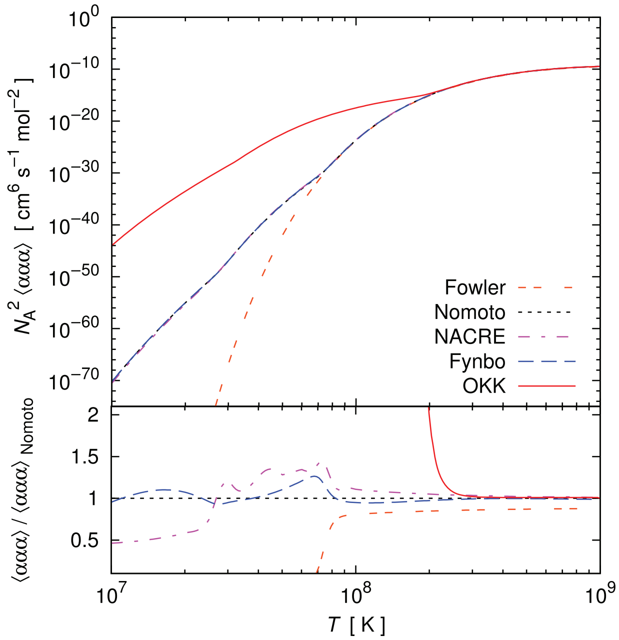

Fig. 1. Triple-α reaction rates as a function of temperature. "Fowler," "Nomoto," "NACRE," "Fynbo," and "OKK" are the 3α reaction rates taken from Fowler et al. (1975) [10], Nomoto et al. (1982a) [6], NACRE (Angulo et al. 1999) [8], Fynbo et al. (2006) [9], and Ogata et al. (2009) [7], respectively. The top panel shows thermonuclear reaction rates and the lower panel shows the ratios with respect to "Nomoto." $\langle\alpha\alpha\alpha\rangle$ is the reaction rate per three α particles.

The astrophysical S-factor at this energy, $S(300)$, is estimated to be 100 keV·b and 230 keV·b from Refs. [11] and [12], respectively. In particular, the latter rate, referred to as CF85, has been adopted to explore supernova nucleosynthesis and the final results seem to give a good agreement with the observation of SN 1987A [3]. Another value has been presented using a different method to determine the cross section, which utilizes the reacion of $^{16}\mathrm{N}(\beta^-)^{16}\mathrm{O}^* \rightarrow {}^{12}\mathrm{C} + \alpha$ and gives $S(300) = 146$ keV·b (hereafter referred to as Bu96) [13]. Although the uncertainty is not so large compared to the triple-α rate as shown in Fig. 2, where the representative rates obtained so far are compared, the effects on the nucleosynthesis are significant [14–17].

It has already been shown that the OKK rate crucially affects the evolutionary tracks of low-mass stars, where the evolution from zero-age main sequence to core He flash/burning for low-, intermediate-, and high-mass stars have been investigated [18,19]. The HR diagram obtained using the new 3α reaction rate disagrees considerably with the observations of low-mass stars; the OKK rate results in the shortening or disappearance of the red giant phase, because helium ignites at a much lower temperature and density compared to the case of the NACRE rate [8]. Furthermore, stellar models in the mass range of $0.8 < M/M_\odot < 25$ were computed and it was confirmed that the OKK rate has significant effects on the evolution of low- and intermediate-mass stars, while its influences on the evolution of massive stars ($M > 10\,M_\odot$) are minimal [20]; the OKK rate is incompatible with observations but for massive stars. If the OKK rate is correct, we must invoke some new physical processes such as rotational mixing [21,22], turbulence [23], dynamical instabilities [24], or other unknown physical effects. On the other hand, the abundances of helium and heavier elements in globular clusters are open to dispute [25], which may change the scenario of the stellar evolution of low-mass stars.

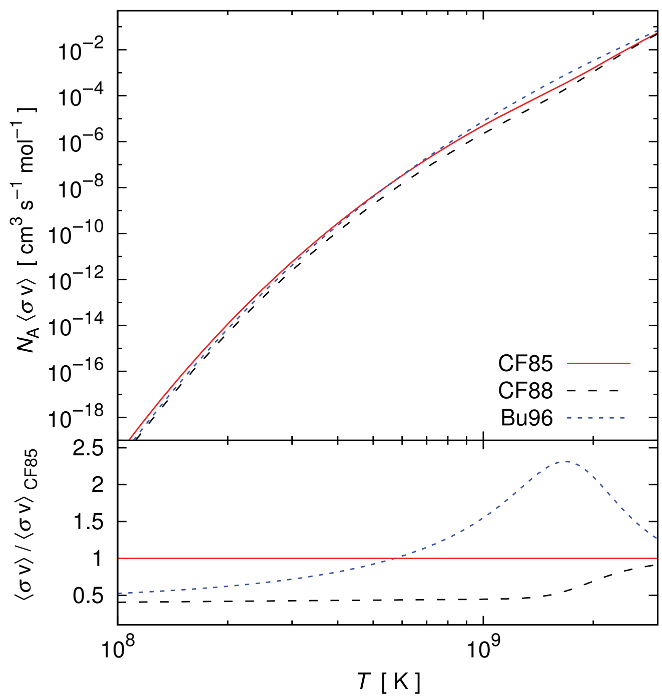

Fig. 2. Thermonuclear reaction rates for $^{12}C(\alpha, \gamma)^{16}O$ as a function of temperature. The abbreviations "CF85," "CF88," and "Bu96" are taken from Caughlan et al. (1985) [12], Caughlan and Fowler (1988) [11], and Buchmann et al. (1996a) [13], respectively. The upper panel shows thermonuclear reaction rates per particle and the lower panel shows the ratios with respect to "CF85."

Apart from appearances of observations, we can see the effects of the OKK rate on stellar evolution from the ignition properties. A helium core flash is triggered if the nuclear energy generation rates (ε_n) become significantly larger than the neutrino energy loss rates (ε_ν). We can understand clearly that helium ignition under the degenerate condition ($\varepsilon_n = \varepsilon_\nu$) occurs at considerably lower temperature and density points compared with the previous case [26]. The effects of the OKK rate on the evolution of accreting compact stars have been studied: the ignition property for accreting white dwarfs [26] and X-ray bursts on accreting neutron stars [27]. It was also found that the s-process using the OKK rate during core He-burning is very inefficient compared to the case with the previous 3α rates. However, the difference in overproduction is found to be almost compensated by the subsequent C-burning, and the overproduction level is not different as a whole for the two distinctly different 3α rates. Therefore, the weak s-process in massive stars does not testify to the validity of the new rate. Tur et al. [15] investigated the dependence of the s-process and post-explosive nucleosynthesis on $\pm 2\sigma$ experimental uncertainties of 3α and $^{12}C(\alpha, \gamma)^{16}O$ reaction rates. However, the impact of such large theoretical uncertainties of 3α rates invoked by the OKK rate [7] with those of $^{12}C(\alpha, \gamma)^{16}O$ have not been explored on the supernova yields of a massive star.

In the present paper, we investigate the effects of both 3α and $^{12}C(\alpha, \gamma)^{16}O$ rates on the production of the possible isotopes during the evolution of a massive star of 25 $M_\odot$ and its supernova explosion. In Sect. 2, the evolution of massive stars of 20 $M_\odot$ and 25 $M_\odot$ stars are presented, where the effects of the rates on the evolution and the nucleosynthesis are discussed. The method of calculation for the supernova explosion of 25 $M_\odot$ stars is presented in Sect. 3. The results of nucleosynthesis and some discussions are also given by comparing with solar system abundances. In Sect. 4, the most suitable combination of the reaction rates is deduced and the remaining problems are presented.

2. Nucleosynthesis at the presupernova stages

The triple-α and $^{12}C(\alpha, \gamma)^{16}O$ rates are the key nuclear reaction rates concerning He-burning in massive star evolution. As a consequence, explosive nucleosynthesis and the resulting supernova yields of a massive star would be influenced seriously by the two rates. We select four combinations from the available nuclear data for the two rates, that is, Fynbo–CF85, Fynbo–Bu96, OKK–CF85, and OKK–Bu96, which must cover the possible uncertainties inherent to the experiments and/or theories. The stellar evolutionary code is almost the same as Ref. [2,3] but for the revised reaction rates [11]. To study detailed abundance distributions including s-nuclei, we perform a post-process nucleosynthesis calculation with a large nuclear reaction network using the same methods as described in Ono et al. [30] and Kikuchi et al. [31].

Let us explain our nuclear reaction network for completeness. Our network contains 1714 nuclei from neutron and proton to uranium isotopes up to ^{241}U linked through particle reactions and weak interactions [30,32]. The reaction rates are taken from the JINA REACLIB compilation [33], where updated nuclear data has been included for charged particle reactions and (n, γ) cross sections after those of Bao et al. [34]. The finite temperature and density dependences of beta decay and electron capture rates for nuclei above ^{59}Fe are included based on Ref. [35].

After helium core formation, gravitational contraction leads to ignition by the 3α reaction. Near the end of core He-burning, the $^{12}C(\alpha, \gamma)^{16}O$ reaction begins to operate significantly. As a consequence, the production of ^{12}C and ^{16}O proceeds appreciably and these elements should become the main products after core He-burning in all massive stars. From core C-burning to the end of core oxygen burning, carbon continues to decrease little by little due to shell burnings. This fact is almost universal from zero to solar metallicity stars, because massive stars form helium cores after hydrogen burning, except for extremely massive stars which could induce pair instability supernovae [36].

Figure 3 shows the evolutionary tracks for the density and temperature at the center in the cases of 20 $M_\odot$ and 25 $M_\odot$ stars, where the Fynbo–CF85 and OKK–CF85 rates are adopted. The evolution with respect to the 25 $M_\odot$ stars leads to presupernova stages for both rates. The situation becomes rather complex if we examine the evolution of the 20 $M_\odot$ stars. For the case of Fynbo–CF85, the presupernova stage is attained as before [2,3]. For the case of OKK–CF85, Si-ignition barely occurs and the evolution would lead to the formation of an Fe-core. In the present study, we stopped the calculation of Si-burning; since the shell burnings of O, Ne, and C are often very active, the computation becomes difficult to continue. The details of the tracks depend on both the strength of the shell burnings and the extension of the convective mixing. Finally, the presupernova stages are attained, as seen in Fig. 4 for the 25 $M_\odot$ stars. On the other hand, we find that the presupernova stage cannot be obtained for a 20 $M_\odot$ star with the Fynbo–Bu96 model, but instead the star begins to cool, as seen in Fig. 4; the central region cannot attach the ignition curve of Si on the density–temperature plane.

In general, whether nuclear ignition occurs or not can be judged from the temperature to which the burning region heats up. If the temperature does not reach the ignition temperature, the region begins to cool. The central temperature depends significantly on the strength of shell burnings. In particular, the production of carbon at the end of core helium burning is closely related to the subsequent evolution of the stars, because the carbon shell determines the boundary between the inner core of the carbon–oxygen core and the helium envelope. Furthermore, active carbon burning hinders the increase of the central temperature and leads to a delay in gravitational contraction. Therefore, the formation of the Fe-core is doubtful if we adopt the combination of the reaction rates of OKK–CF85 or Fynbo–Bu96, because the central temperature is just around the ignition line for Si.

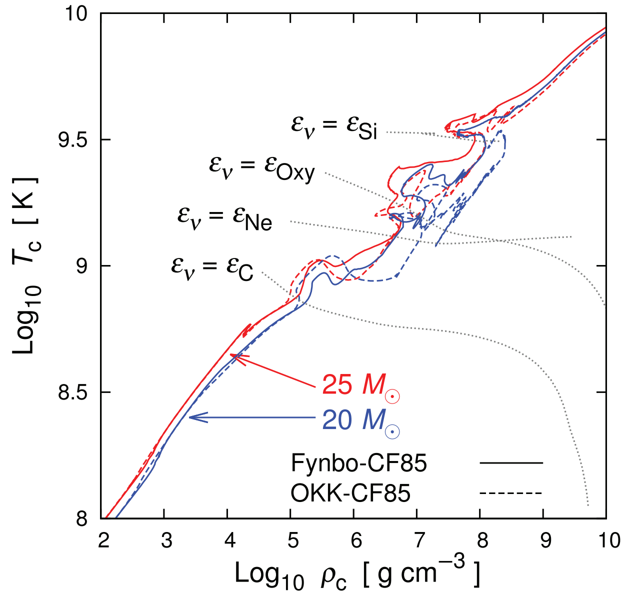

Fig. 3. Evolutionary paths on the plane for the density and the temperature at the center of the 20 $M_\odot$ and 25 $M_\odot$ stars. The solid and dashed lines are the results from the Fynbo and OKK rates using CF85, respectively. The ignition curves (dotted lines) show the beginning of C-, Ne-, O-, and Si-burning, where the neutrino loss rates are equal to the nuclear energy generation rates.

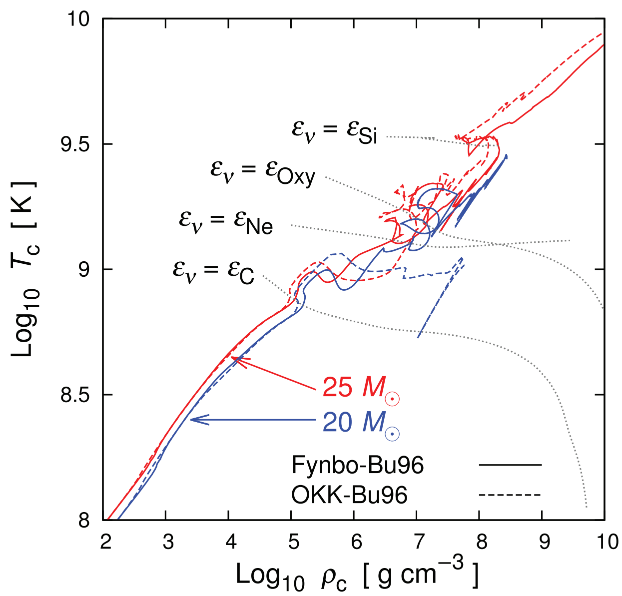

Fig. 4. As Fig. 3 except for the reaction rate Bu96 of $^{12}C(\alpha, \gamma)^{16}O$.

We note that once the ignition of silicon begins, an Fe-core forms at the center and gradually grows towards the Chandrasekhar mass [2]. Although the model of OKK–CF85 may not be excluded as a progenitor, the evolutionary scenario will become complex compared to the previous scenario [2,3]. It should be noted that the evolution becomes very complex for massive stars whose masses are less than 20 $M_\odot$; this can be inferred from Figs. 3 and 4. The reaction rates OKK–Bu96 drastically change the evolutionary history of 20 $M_\odot$ stars compared to the case with Fynbo–CF85, and the evolutionary path resembles a star of around 10 $M_\odot$, where the nuclear ignition for neon burning does not occur

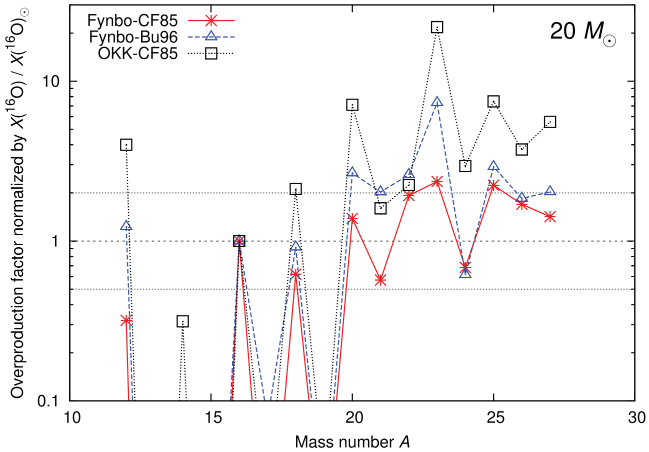

Fig. 5. The overproduction factors of nuclei lighter than $A = 27$ in the 20 $M_\odot$ stars at the start of Si-burning, normalized by the abundance of ^{16}O. The asterisks, triangles, and squares are the results from the Fynbo–CF85, Fynbo–Bu96, and OKK–CF85 models, respectively. The two dotted lines show the values whose ratios to the normalized overproduction factors of ^{16}O are two or one-half.

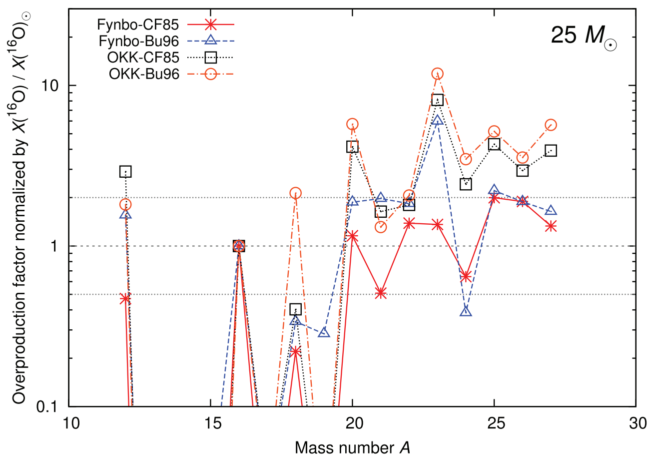

Fig. 6. As Fig. 5 but for 25 $M_\odot$ stars at the presupernova stages using all combinations of reaction rates.

at the center [37]. As a consequence, the evolutionary scenario of less massive stars ($M \leq 20\,M_\odot$) would change significantly.

Figures 5 and 6 illustrate the overproduction factors $X(i)/X(i)_\odot$, where $X(i)$ denotes the mass fraction of element i, concerning main products ($12 \leq A \leq 27$) normalized by the oxygen one, $X(^{16}\mathrm{O})/X(^{16}\mathrm{O})_\odot$. The two dotted lines show the values whose ratios to the normalized overproduction factor of ^{16}O are two or one-half. Figure 5 shows the case of the 20 $M_\odot$ stars at the beginning of Si-burning for three combinations of reaction rates; it is noted that the abundances referred to in the panel do not change appreciably after Si-burning. Figure 6 shows the case of the 25 $M_\odot$ stars at the presupernova stages for the four combinations. As a whole, the Fynbo–CF85 model gives a reasonable range of abundance ratio compared to solar abundances, except for ^{12}C which is supplied through ejection from AGB stars [38,39]. For other models, however, the overproduction factors of some elements are beyond the values whose ratios to those of oxygen are two (upper dotted lines).

In Figs. 5 and 6, the models except for Fynbo–CF85 produce a significantly large amount of ^{20}Ne, ^{23}Na, and ^{24}Mg because of strong C-burning. Since these elements remain in the burning layers of

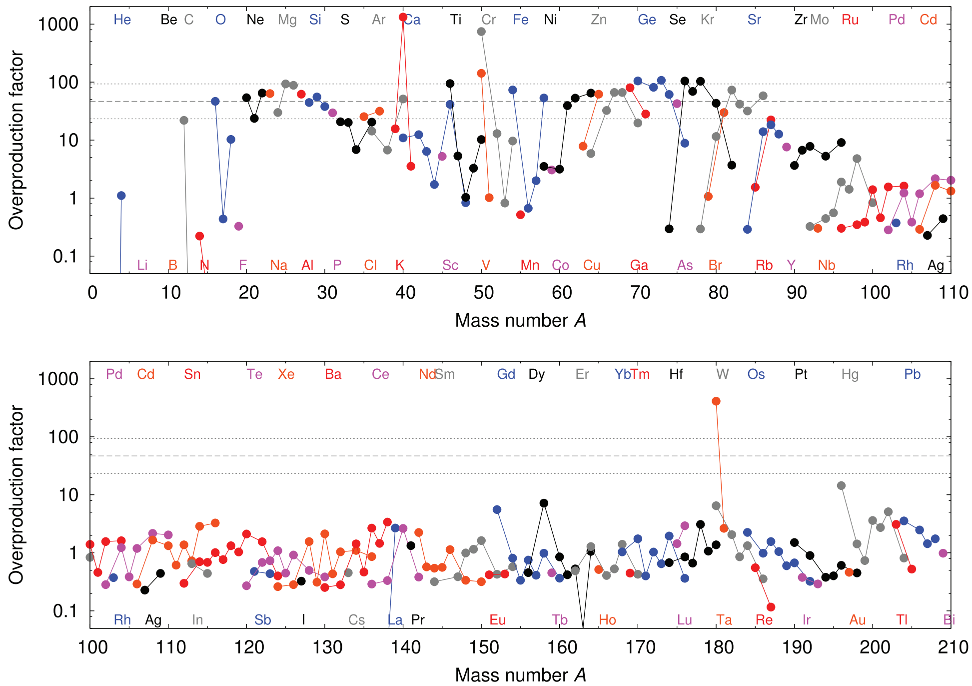

Fig. 7. Overproduction factors of all stable nuclei of $A < 210$ for the Fynbo–CF85 model at the presupernova stage for a 25 $M_{\odot}$ star. The dotted lines denote the values whose ratios to the overproduction factor of ^{16}O are two or one-half. The dashed line shows the value of ^{16}O.

O and Ne, significant amounts will survive even after the shock wave propagation during the explosion. The amounts can be obtained by simulating the explosion. The fate of a star towards Fe-core formation is still uncertain due to convective mixing, even under the assumption of spherical symmetry [2,3]. However, we have succeeded in the stellar evolutionary calculations until the beginning of Fe-core collapse only for the 25 $M_{\odot}$ star for the four reaction sets, as seen in Figs. 3 and 4. It is desirous to adopt the complete set of presupernova models to examine the effects of four sets of reaction rates on nucleosynthesis. Therefore, we show the nucleosynthesis after the supernova explosions in the next section by concentrating on the 25 $M_{\odot}$ stars.

In Kikuchi et al. [31], we have already investigated the effects of the OKK rate on the production of the s-process nucleosynthesis for a 25 $M_{\odot}$ star. However, the calculation was stopped at the end of central C-burning. Therefore, we can discuss the s-process nucleosynthesis after central C-burning in the present paper. Overall, at the end of C-burning, the overproduction factors of s-nuclei are roughly consistent with those of Ref. [31]. After C-burning, neutron irradiations in C-burning shells enhance the overproduction factors of some s-nuclei by a factor of 3–4 (for ^{80}Kr, even greater than 10) compared to those at the end of C-burning. The significant enhancement of the s-process elements during the later evolutionary stages has already been claimed by Tur et al. [15]. We have confirmed that the level of the enhancement of overproduction factors due to the later burning stages is roughly consistent with that in the Ref. [15]. Since s-elements become seeds of p-process nucleosynthesis in massive stars and the p-process has been believed to occur during a supernova explosion at the bottom of the oxygen-rich layer, the amount of s-elements that can survive is crucial to discussing the nucleosynthesis of p-elements in supernovae.

Let us examine the nucleosynthesis for nuclei above $A > 40$, other than s-nuclei, concerning 25 $M_{\odot}$ stars. In Fig. 7, the Fynbo–CF85 model gives significant overproductions compared to the initial solar abundances for the neutron-rich nuclei of ^{40}K (1325), ^{50}V (142), ^{50}Cr (744), and ^{180}Ta (410), where the numerals inside the brackets are the overproduction factors with respect to their initial values. In the present case, we summed the mass of each nucleus above approximately 1.5 $M_\odot$, which corresponds to the "mass cut" described in Sect. 3. On the other hand, other models do not produce much of those nuclei except for ^{40}K, where the overproduction factors are 1092, 1347, and 1281 for Fynbo–Bu96, OKK–Bu96, and OKK–CF85, respectively. For other nuclei, three models result in overproduction factors less than 100. Exceptionally, Fynbo–Bu96 and OKK–Bu96 models give overproduction factors of 142 for ^{76}Se and 141 for ^{50}Cr, respectively. It is noted that the first three nuclei (^{40}K, ^{50}V, ^{50}Cr) are the products after the oxygen burning. As seen in Fig. 6, oxygen production overwhelmed carbon production after He-burning for the Fynbo–CF85 model. As a consequence, the model tends to considerably overproduce these nuclei, as can be seen in Fig. 7. ^{180}Ta is mainly produced by the (γ, n) reaction of ^{181}Ta. The overproduction of ^{180}Ta for Fynbo–CF85 is attributed to the enhanced (γ, n) reaction owing to higher temperatures during the later evolutionary stages, as seen in Fig. 3. After the supernova explosion, these nuclei around the bottom of the oxygen-rich layers are destroyed and/or transformed to other nuclei. Therefore, except for some nuclei, overproductions are decreased, as is discussed in the next section. In the following section, we focus on the nucleosynthesis of 25 $M_\odot$ stars, because we can succeed in getting the presupernova models for the four models of Fynbo–CF85, Fynbo–Bu96, OKK–CF85, and OKK–Bu96. The more massive stars will result in straightforward evolution toward Fe-core collapse. The less massive stars experience rather complex evolutions, as inferred from Fig. 4.

3. Supernova nucleosynthesis and overproduction factors

We investigate the production of the elements for massive stars of 25 $M_\odot$. To estimate the amount of material ejected into the interstellar medium from the exploding star, we perform a simulation of the supernova explosion. The procedure of this calculation has been described in a preceding study [40]. Therefore, we explain the calculation method briefly. The equations of hydrodynamics are as follows, using the Lagrange mass coordinate m (e.g., Ref [41]):

$$\frac{\partial V}{\partial t} - \frac{\partial\left(4\pi r^2 v\right)}{\partial m} = 0, \tag{1}$$

$$\frac{\partial q}{\partial t} + \frac{\partial\left(4\pi r^3 p\right)}{\partial m} = v^2 + \frac{3p}{\rho} - \frac{Gm}{r}, \tag{2}$$

$$\frac{\partial e}{\partial t} + \frac{\partial\left(4\pi r^2 v p\right)}{\partial m} = H. \tag{3}$$

Equation (1) describes the equation of continuity with the specific volume $V = \rho^{-1}$, where r and v are the radius and velocity, respectively. Equation (2) is the conservation of momentum, where p is the pressure, q is the scalar specific momentum described as $q = \boldsymbol{v} \cdot \boldsymbol{r}$, and G is the gravitational constant. Equation (3) gives the equation of energy conservation; e is the specific energy expressed as $e = \frac{v^2}{2} + U - \frac{Gm}{r}$, where U is the specific internal energy, and H is the heating term for the nuclear energy generation (energy per unit mass per unit time).

Concerning the initial models, we adopt the presupernova models obtained in Sect. 2. The input physical values are the temperature, density, pressure, and chemical compositions. Our hydrodynamical code includes an α-network which contains 13 species: ^{4}He, ^{12}C, ^{16}O, ^{20}Ne, ^{24}Mg, ^{28}Si, ^{32}S, ^{36}Ar, ^{40}Ca, ^{44}Ti, ^{48}Cr, ^{52}Fe, and ^{56}Ni [42]. The calculation continues until the time of around 300 s

Table 1. Physical quantities for the explosion models. The Fe-core mass M_{Fe} and mass cut M_{cut} are values in units of $M_{\odot}$. The injected energy E_{in} is in units of 10^{51} erg.

Models	Fynbo–CF85	Fynbo–Bu96	OKK–CF85	OKK–Bu96
M_{Fe}	1.36	1.25	1.24	1.34
E_{in}	1.44	1.06	1.30	1.16
M_{cut}	1.70	1.35	1.46	1.53

when the shock wave reaches the surface of the helium core; at the same time the explosion energy is calculated.

The explosion is initiated by injecting thermal energy around the surface of the Fe-core. To see the effects of different combinations of the reaction rates, we fixed the explosion energy and ejected ^{56}Ni mass to be 1.0×10^{51} erg and 0.07 $M_{\odot}$, respectively. We adopt these values from SN 1987A [42] as a core-collapse supernova explosion model. The injected energy is adjusted to obtain an explosion energy of 1.0×10^{51} erg. We note that the locations in the Lagrange mass coordinate at which the thermal energies are injected, i.e. the surfaces of the Fe-cores, are different for each model, because different combinations of the reaction rates result in different Fe-core masses. After the nucleosynthesis calculation described later, we redefine a boundary between the ejecta and the compact object which is a so-called "mass cut" (M_{cut}) to obtain 0.07 $M_{\odot}$ ^{56}Ni in the ejecta. It is assumed that the material between M_{Fe} and M_{cut} ($M_{\mathrm{Fe}} < M_{\mathrm{cut}}$) falls into the compact object. Table 1 shows the physical quantities concerning the explosion, that is, the mass of the Fe-core M_{Fe}, the injected energy E_{in}, and the mass cut M_{cut}.

Using the results of the density and temperature evolution during the shock propagation, we calculate nucleosynthesis with a large nuclear reaction network. The calculations are performed until 10^{17} s after the explosion, which leads to stable nuclei (we extrapolate the density and temperature after 300 s to continue the nucleosynthesis calculation assuming an adiabatic expansion). The reaction network is almost the same as that of the evolution calculation with 1714 species, but we add proton-rich elements around the Fe group nuclei for explosive nucleosynthesis, whose network includes 1852 nuclear species.

To compare the results with observations, overproduction factors, $X(i)/X(i)_{\odot}$, are considered. We show the results for stable elements lighter than $A = 210$ in Fig. 8 (Fynbo–CF85), Fig. 9 (Fynbo–Bu96), Fig. 10 (OKK–CF85), and Fig. 11 (OKK–Bu96). We classify the nuclei produced into two groups: one is the nuclei produced in mainly massive stars and ejected by the explosions (nuclei of $20 \leq A \leq 32$ and weak s-nuclei of $60 < A < 90$) and the other is p-nuclei. The underproduced nuclei are contributed by other astrophysical sites. Nuclei of $A < 20$ are also synthesized in low- and intermediate-mass stars. The intermediate-mass stars yield the main s-nuclei ($A = 90$–210) during the AGB star phase [43–45]. Type Ia supernovae synthesize the nuclei between Cl and the Fe group nuclei. R-nuclei could be produced by neutron star mergers [46–49], magnetorotationally driven supernovae [32,50], and/or neutrino-driven supernovae [51]. In the following sections (Sect. 3.1 and 3.2), we discuss the overproduction factors by focusing on different results due to the four sets of reaction rates.

3.1. *Overproduction factors for* $A \leq 110$

Here, we consider overproduction factors averaged in the ejecta at the time of 10^{17} s after the explosion. In Figs. 8–11, the overproduction factors for the Fynbo–CF85, Fynbo–Bu96, OKK–CF85, and

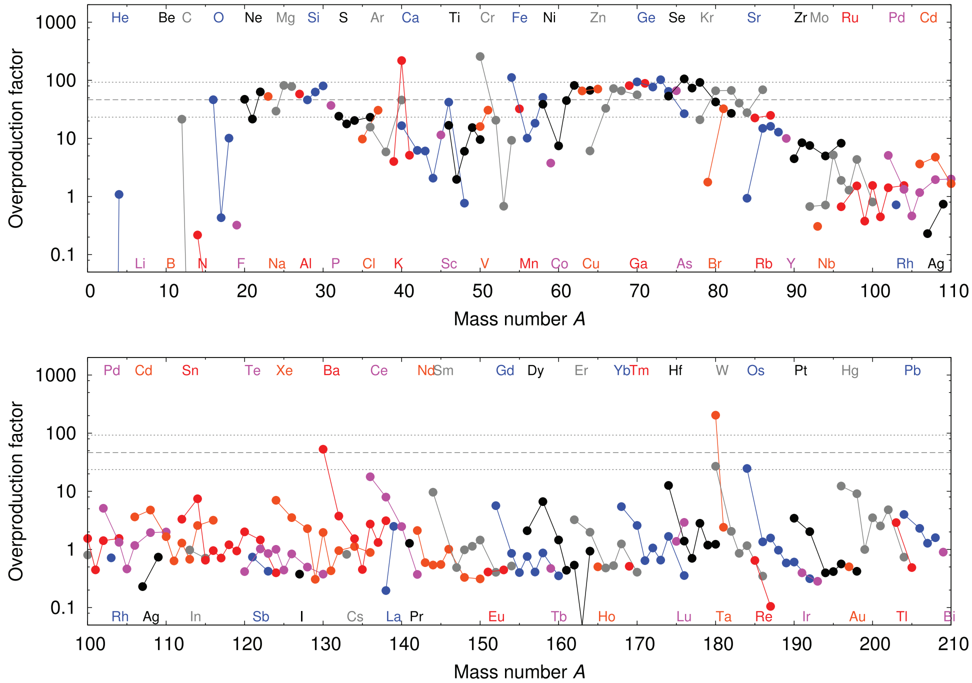

Fig. 8. Overproduction factors of all stable nuclei of $A < 210$ for the Fynbo–CF85 model at 10^{17} s after the explosion. The dotted lines denote the values whose ratios to the overproduction factor of ^{16}O are two or one-half. The dashed line shows the value of ^{16}O.

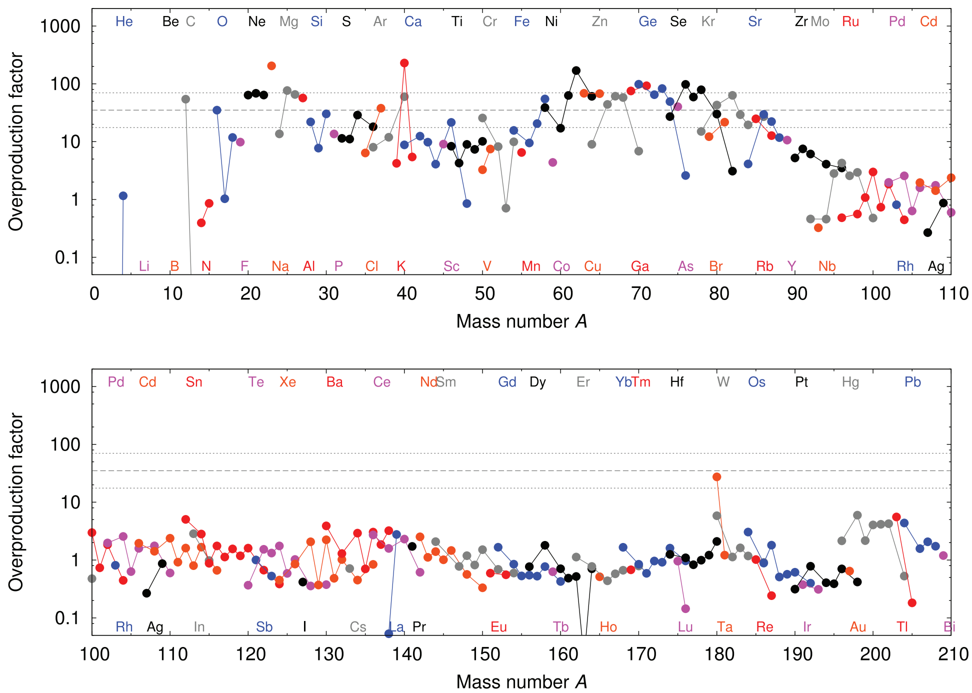

Fig. 9. As Fig. 8 but for the Fynbo–Bu96 model.

OKK–Bu96 models are shown. The dotted lines indicate the values whose ratios to the overproduction factor of ^{16}O are two or one-half. If the ratios are found between the values of one-half and two, they would be consistent with solar abundances. The Fynbo–CF85 model reproduces well the solar system abundances of $20 \leq A < 32$, where ^{21}Ne could be barely in the range. For the Fynbo–Bu96

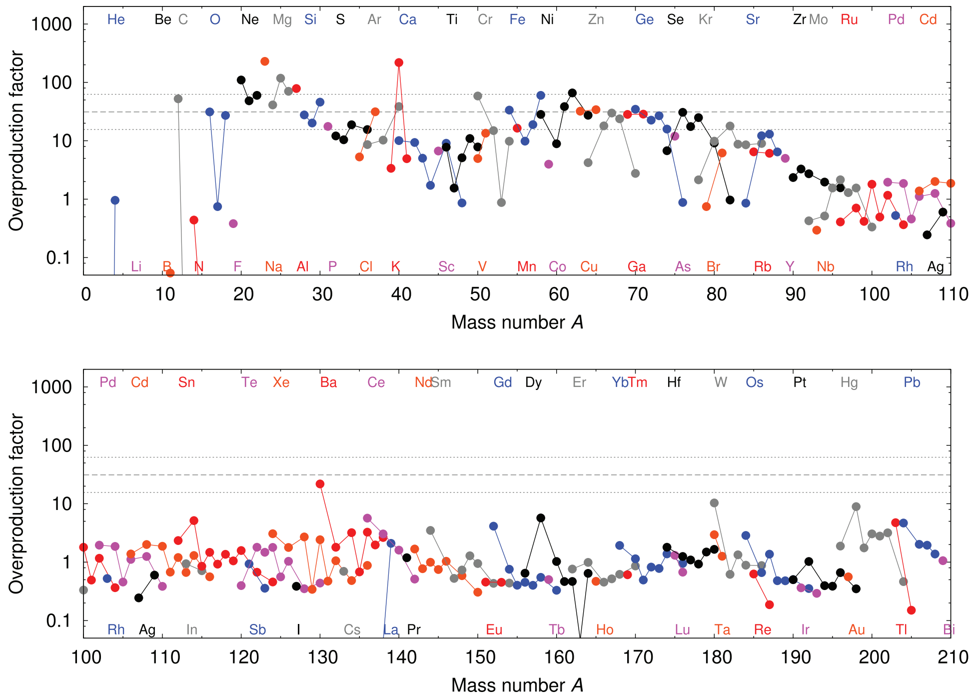

Fig. 10. As Fig. 8 but for the OKK–CF85 model.

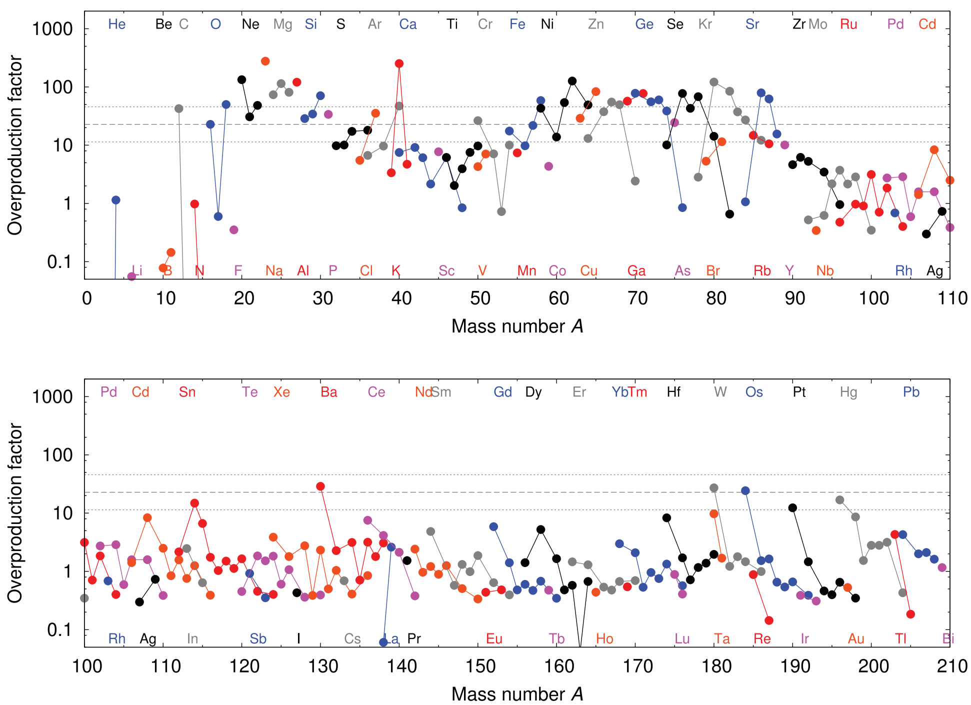

Fig. 11. As Fig. 8 but for the OKK–Bu96 model.

model, isotopes of $20 \leq A < 32$ are well reproduced except for ^{23}Na and ^{24}Mg. For the OKK–CF85 model, ^{20}Ne, ^{23}Na, ^{25,26}Mg, and ^{27}Al are beyond the values whose ratios to that of ^{16}O are two (these nuclei are synthesized from ^{12}C+^{12}C reactions). ^{22}Ne, which is produced from ^{14}N, and nuclei of

$27 \le A \le 32$ are reproduced well enough. For the OKK–Bu96 model, those of $20 \le A \le 27$ are extremely overproduced but $28 \le A < 32$ well reproduced.

The weak s-process produced the elements up to $A = 90$ in all four models. Some s-nuclei are destroyed by the explosion but almost all the other s-nuclei survived. Therefore, the yields after the explosion are nearly the same as those in the presupernova stage. The overproduction factors for the OKK–CF85 model are the least enhanced among the four models, and those of the OKK–Bu96 model are the most enhanced, especially around $A = 90$. These differences are related to He- and C-burning, which are crucially important for the weak s-process [31]. For the OKK–Bu96 model, ^{12}C is produced appreciably compared to the other three models, which leads to the increase in neutron production during C-burning.

3.2. *Overproduction factors of p-nuclei*

In general, p-nuclei are produced by way of photodisintegration of seed s-nuclei during a supernova explosion. The condition for an adequate p-process to occur has been found. The relationship between synthesized p-nuclei and the peak temperature T_{p}, the maximum temperature at each Lagrange mass coordinate during the passage of the supernova shock wave, has been given with the mass number A and neutron number N as follows [52,53]:

(1) $T_{\mathrm{p}} = 2 \times 10^9$ K: (γ, n) reactions dominate the p-process. A small fraction of the heaviest and most fragile seed nuclei $N > 82$ are destroyed and produce heavy p-nuclei ($N > 82$, $A > 140$).
(2) $T_{\mathrm{p}} = 2$–2.4×10^9 K: (γ, α) and/or (γ, p) reactions also become active ($N > 82$) and heavy p-nuclei are synthesized through the (γ, n) reactions.
(3) $T_{\mathrm{p}} = 2.4$–2.6×10^9 K: p-nuclei of $N > 82$ are destroyed by photodisintegration. After the reactions freeze out, the elements become stable nuclei by way of β^+ decay. Some intermediate p-nuclei are produced.
(4) $T_{\mathrm{p}} = 2.7$–3.0×10^9 K: Seed nuclei of $50 < A < 82$ are photodisintegrated and most intermediate ($50 < N < 82$) p-nuclei are synthesized.
(5) $T_{\mathrm{p}} > 3 \times 10^9$ K: All heavy seed nuclei are destroyed. Light p-nuclei ($N < 50$) are produced.

In Fig. 12, the overproduction factors of all p-nuclei after the explosion are plotted. Most p-nuclei are produced in descending order of the Fynbo–CF85, OKK–Bu96, OKK–CF85, and Fynbo–Bu96 models. To consider the reason for the differences among the models seen in Fig. 12, we take into account the relationship between the p-process and the peak temperature. We define the so-called p-process layers (hereafter PPLs) [52] as the regions with peak temperatures of (2–3.5) $\times 10^9$ K. Peak temperatures against the Lagrange mass coordinate are shown in Fig. 13. The size of the PPL for the Fynbo–CF85 model is equal to 0.65 $M_\odot$, the largest amount among the four models. Towards the gravitational collapse, the Fynbo–CF85 model forms gradually higher temperature and density regions through the stellar evolution. The sizes of PPLs for other models are 0.27 $M_\odot$ (OKK–Bu96 model), 0.24 $M_\odot$ (OKK–CF85 model), and 0.19 $M_\odot$ (Fynbo–Bu96 model). Therefore, the overproductions of p-nuclei are in descending order of the sizes of the PPLs. Since peak temperatures attained by the shock wave propagation depend on the density distribution or the stellar radius at the presupernova stage, the amount of p-nuclei is affected by the gravitational contraction and/or shell burnings. It is noted that isotopes of ^{92,94}Mo and ^{96,98}Ru are still underproduced. Furthermore, both ^{113}In and ^{115}Sn are produced to some extent. These nuclei have been known to be significantly underproduced [52]. Variations of production of p-nuclei depend on the survived seed s-nuclei. The

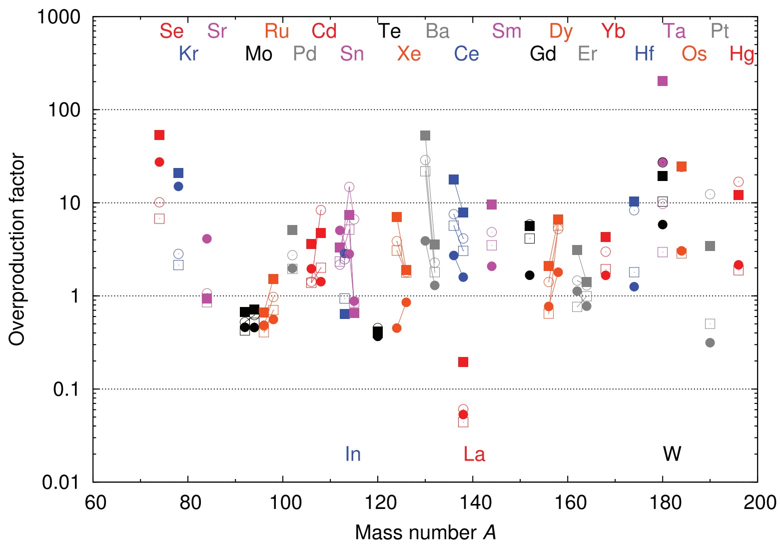

Fig. 12. Overproduction factors of all p-nuclei against the mass number A at the time of 10^{17} s after the explosion. All unstable parent nuclei are decayed to stable daughter p-nuclei. Filled squares are the results of the Fynbo–CF85 model, filled circles are those of Fynbo–Bu96, empty squares are those of OKK–CF85, and empty circles are those of OKK–Bu96.

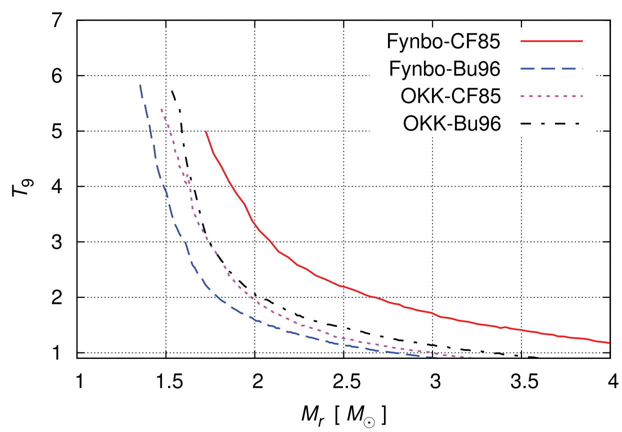

Fig. 13. Peak temperatures against mass coordinate M_r. T_9 denotes $T/(10^9\,\mathrm{K})$. The solid line is the result of the Fynbo–C85 model, the dot-dashed line is OKK–Bu96, the dotted line is OKK–CF85, and the dashed line is OKK–Bu96. p-process layers (PPLs) [52] are defined as the regions with the peak temperature of $(2–3.5) \times 10^9$ K.

difference in overproduction of the above p-nuclei compared to the previous study [52] is attributed to the detailed calculations of the nucleosynthesis during the stellar evolution.

3.3. *Summary of nucleosynthesis*

We have shown the supernova nucleosynthesis for 25 $M_\odot$ stars using presupernova models which are the results of the stellar evolution calculations with four sets of 3α and ^{12}C(α, γ)^{16}O reaction rates and the postprocessing nucleosynthesis with the large nuclear reaction network. We emphasize that the final results of supernova nucleosynthesis depend not only on the explosion episode but also on the history of stellar evolution towards the Fe-core collapse. Generally speaking, the models with the OKK rate overproduce the isotopes of Ne, Mg, and Na beyond an acceptable level; these originate from the burning of ^{12}C and subsequent shell burnings. For all models, the amount of s-nuclei does not change appreciably compared to that of the presupernova stage. As a consequence, He- and C-burnings are significantly important for the weak s-process. On the other hand, the distribution and amount of p-nuclei depend on peak temperatures and the size of PPLs, which are affected by the stellar evolution path, i.e., 3α and ^{12}C$(\alpha, \gamma)^{16}$O reaction rates. Although each overproduction factor is influenced to some extent, the heavy element nucleosynthesis is not affected appreciably by the triple-α and ^{12}C$(\alpha,\gamma)^{16}$O rates as a whole. Therefore, it is difficult to testify to the validity of the two reaction rates by the s- and p-process elements.

4. Discussions

We have investigated the effects of 3α and ^{12}C$(\alpha, \gamma)^{16}$O reaction rates on the production of the supernova yields in a massive star of 25 $M_\odot$, where four combinations of the representative reaction rates are selected and incorporated in the nuclear reaction network. Since the evolutionary code used in the present study is almost the same as Refs. [2,3] but for the reaction rates, the differences in the evolutionary path should come from the extent of the convective mixing originated from nuclear burnings due to the different reaction rates. For example, the stellar evolutionary path of 20 $M_\odot$ is seriously affected if we adopt the combination of OKK–Bu96 reaction rates, because the carbon produced induces strong carbon-shell burnings. Concerning the 25 $M_\odot$ star, we can perform the evolutionary calculations till the presupernova stages and obtain the Fe-cores just before the collapse for all the combinations of reaction rates. As a consequence, we can recognize significant effects on supernova yields. 1) The distribution of abundance before the core collapse becomes very different for each model. 2) The supernova explosion results in distinctive yields if we compare them with the solar system abundances. The Fynbo–CF85 model can reproduce the solar values well for $A < 40$ and it becomes difficult to reproduce the solar ones in ascending order of the Fynbo–Bu96, OKK–CF85, and OKK–Bu96 models, as seen in Figs. 8–11. It should be noted that ^{23}Na is much overproduced except for the Fynbo–CF85 model. Therefore, Fynbo–CF85 is the most suitable combination of the 3α and ^{12}C$(\alpha,\gamma)^{16}$O reaction rates to be compatible with the solar system abundances. It is noted that the CF85 rate for the ^{12}C$(\alpha,\gamma)^{16}$O reaction is considered to be the upper limit within the experimental uncertainties.

As for the heavy nuclei beyond the iron group elements, it is unclear how to judge the compatibility with the observations. The problem of underproduction of p-nuclei remains when compared to the solar values [54]. There exist crucial problems concerning the stellar models, for which we do not have a satisfactory theory of convective mixing. Since we have adopted the Schwartzschild criterion for convection, the convection tends to occur rather easily compared to the Ledoux criterion. Furthermore, the extent of convective mixing is not well known, where convection itself is closely related to nuclear burnings [24]. We should note that these problems arise from the assumption that the stars are spherically symmetric and at present any satisfactory calculation of non-spherical stellar evolution does not exist [56,57]. Although the helium core is assumed to be 8 $M_\odot$, the actual star begins its evolution from the main-sequence stage with a hydrogen-rich envelope. If we consider the hydrogen-rich envelope, we will worry about the mass loss rate which brings out uncertain parameters [58]. As far as the approach of the helium star is concerned, our results would be legitimate because, after the end of hydrogen burning, a star forms the helium core with a clear boundary between the core and envelope, which is equivalent to the helium star [1]. Observationally, our approach has been supported by observations of light curves [42,59] and supernova nucleosynthesis [3,40] as far as SN 1987A is concerned. Therefore, at present our conclusion could be accepted even if the unsatisfactory theory of convection lies under the calculation of stellar evolution.

Acknowledgements

We thank Dr Masahiro Machida, Takashi Teranishi, and Kenzo Arai for helpful discussions. This work has been supported in part by a Grant-in-Aid for Scientific Research (24540278) of the Ministry of Education, Culture, Sports, Science, and Technology of Japan.

References

[1] D. Sugimoto and K. Nomoto, Space Sci. Rev. **25**, 155 (1980).
[2] K. Nomoto and M. Hashimoto, Phys. Rep. **163**, 13 (1988).
[3] M. Hashimoto, Prog. Theor. Phys. **94**, 663 (1995).
[4] K. Nomoto, Astrophys. J. **253**, 798 (1982).
[5] K. Nomoto, Astrophys. J. **257**, 780 (1982).
[6] K. Nomoto, F.-K. Thielemann, and S. Miyaji, Astron. Astrophys. **149**, 239 (1985).
[7] K. Ogata, M. Kan, and M. Kamimura, Prog. Theor. Phys. **122**, 1005 (2009).
[8] C. Angulo et al. Nucl. Phys. A **656**, 3 (1999).
[9] H. O. U. Fynbo et al., Nature **433**, 136 (2005).
[10] W. A. Fowler, G. R. Caughlan, and B. A. Zimmerman, Ann. Rev. Astron. Astrophys. **13**, 69 (1975).
[11] G. R. Caughlan and W. A. Fowler, Atomic Data and Nuclear Data Tables **40**, 283 (1988).
[12] G. R. Caughlan, W. A. Fowler, M. J. Harris, and B. A. Zimmerman, At. Data Nucl. Data Tables **32**, 197 (1985).
[13] L. Buchmann, R. E. Azuma, C. A. Barnes, J. Humblet, and K. Langanke, Phys. Rep. C **54**, 354 (1996).
[14] C. Tur, A. Heger, and S. M. Austin, Astrophys. J. **671**, 821 (2007).
[15] C. Tur, A. Heger, and S. M. Austin, Astrophys. J. **702**, 1068 (2009).
[16] S. M. Austin, C. West, and A. Heger, Phys. Rev. Lett. **112**, 111101 (2014).
[17] A. Parikh, J. Jose, I. R. Seitenzahl, and F. K. Ropke, Astron. Astrophys. **557**, A3 (2013).
[18] A. Dotter and B. Paxton, Astron. Astrophys. **507**, 1617 (2009).
[19] P. Morel, J. Provost, B. Pichon, Y. Lebreton, and F. Thévenin, Astron. Astrophys. **520**, A41 (2010).
[20] T. Suda, R. Hirschi, and M. Y. Fujimoto1, Astrophys. J. **741**, 61 (2011).
[21] G. Meynet and A. Maeder, Astron. Astrophys. **321**, 465 (1997).
[22] A. Maeder, Astron. Astrophys. **321**, 134 (1997).
[23] C. A. Meakin and D. Arnett, Astrophys. J. **667**, 448 (2007).
[24] N. Smith and W. D. Arnett, Astrophys. J. **785**, 82 (2014).
[25] G. Piotto et al., Astrophys. J. **661**, L53 (2007).
[26] M. Saruwatari and M. Hashimoto, Prog. Theor. Phys. **124**, 925 (2010).
[27] Y. Matsuo et al., Prog. Theor. Phys. **126**, 1177 (2011).
[28] M. Rayet and M. Hashimoto, Astron. Astrophys. **354**, 740 (2000).
[29] N. Prantzos, M. Hashimoto, and K. Nomoto, Astron. Astrophy. **234**, 211 (1990).
[30] M. Ono, M. Hashimoto, S. Fujimoto, K. Kotake, and S. Yamada, Prog. Theor. Phys. **128**, 4 (2012).
[31] Y. Kikuchi, M. Ono, Y. Matsuo, M. Hashimoto, and S. Fujimoto, Prog. Theor. Phys. **127**, 171 (2012).
[32] S. Nishimura, et al., Astrophys. J. **642**, 410 (2006).
[33] R. H. Cyburt et al., Astrophys. J. **189**, 240 (2010).
[34] Z. Y. Bao et al., At. Data Nucl. Data Tables **76**, 70 (2000).
[35] K. Takahashi and K. Yokoi, At. Data Nucl. Data Tables **36**, 375 (1987).
[36] H. Umeda and K. Nomoto, Astrophys. J. **565**, 385 (2002).
[37] K. Nomoto and M. Hahimoto, Prog. Part. Nucl. Phys. **17**, 267 (1986).
[38] W. B. Latter, Astrophys. J. **377**, 187 (1991).
[39] J. S. Greaves and W. S. Holland, Astron. Astrophys. **327**, 342 (1997).
[40] M. Hashimoto, K. Nomoto, and T. Shigeyama, Astron. Astrophys. **210**, L5 (1989).
[41] M. D. Johnston and A. Yahil, Astrophys. J. **285**, 587 (1984).
[42] T. Shigeyama, K. Nomoto, and M. Hashimoto, Astron. Astrophy. **196**, 141 (1988).
[43] O. Straniero, R. Gallino, M. Busso, A. Chieffl, C. M. Raiteri, M. Limongi, and M. Salaris, Astrophys. J. **440**, L85 (1995).

[44] R. Gallino, C. Arlandini, M. Busso, M. Lugaro, C. Travaglio, O. Straniero, A. Chieffl, and M. Limongi, Astrophys. J. **497**, 388 (1998).
[45] C. Arlandini, F. Kappeler, K. Wisshak, R. Gallino, M. Lugaro, M. Busso, and O. Straniero, Astrophys. J. **525**, 886 (1999).
[46] S. Wanajo, Y. Sekiguchi, N. Nishimura, K. Kiuchi, K. Kyutoku, and M. Shibata, Astrophys. J. **789**, L39 (2014).
[47] S. Rosswog, O. Korobkin, A. Arcones, F.-K. Thielemann, and T. Piran, Mon. Not. Roy. Astron. Soc. **439**, 744 (2014).
[48] O. Korobkin, S. Rosswog, A. Arcones, and C. Winteler, Mon. Not. Roy. Astron. Soc. **426**, 1940 (2012).
[49] S. Goriely, A. Bauswein, and H.-T. Janka, Astrophys. J. **738**, L32 (2011).
[50] M. Saruwatari, M. Hashimoto, R. Fukuda, and S. Fujimoto, J. Astrophys. **2013**, 506146 (2013).
[51] S. Wanajo, Astrophys. J. **770**, L22 (2013).
[52] M. Rayet, M. Arnould, M. Hashimoto, N. Prantzos, and K. Nomoto, Astron. Astrophys. **298**, 517 (1995).
[53] N. Prantzos, M. Hashimoto, M. Rayet, and M. Arnould, Astron. Astrophy. **238**, 455 (1990).
[54] M. Rayet, N. Prantzos, and M. Arnould, Astron. Astrophys. **227**, 271 (1990).
[55] O. Koike, M. Hashimoto, K. Arai, and S. Wanajo, Astron. Astrophys. **342**, 464 (1999).
[56] R. Kippenhahn and A. Weigert, *Stellar Structure and Evolution* (Springer-Verlag, Berlin, 1990).
[57] A. Maeder, *Physics, Formation and Evolution of Rotating Stars* (Springer, New York, 2009).
[58] N. Smith, Ann. Rev. Astron. Astrophys. **52**, 487 (2014).
[59] T. Shigeyama, K. Nomoto, M. Hashimoto, and D. Sugimoto, Nature **328**, 320 (1987).